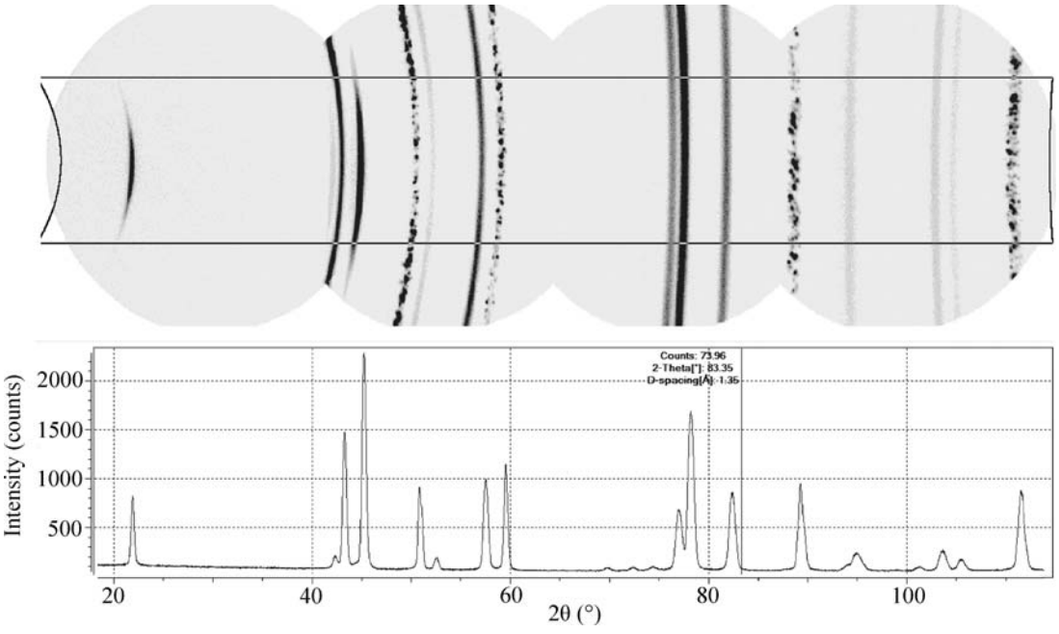

Figure 2.5.16
Diffraction pattern merged from four 2D frames collected from a battery material.

sequential 2θ ranges can be collected. The integrated profiles can then be merged to achieve a large 2θ range. Fig. 2.5.16 shows four 2D frames collected from a battery material with a microgap detector. The slice integration region is defined by two conic lines and two horizontal lines. The diffraction profile integrated from the merged frames is displayed below.

2.5.4.1.3. *Defocusing effect*

A 2D diffraction pattern over a range of 2θ is measured simultaneously with a single incident angle, so the incident angle has to be lower than the minimum 2θ angle. Since the reflected angle cannot always be the same as the incident angle, geometric aberrations are observed. The defocusing effect occurs when the incident angle is lower than the reflection angle. At low incident angles, the incident beam spreads over the sample surface into an area much larger than the size of the original X-ray beam. The observed diffracted beam size is magnified by the defocusing effect if the diffracted beam makes an angle larger than the incident angle. The defocusing effect for reflection-mode diffraction can be expressed as

$$\frac{B}{b} = \frac{\sin\theta_2}{\sin\theta_1} = \frac{\sin(2\theta - \omega)}{\sin\omega}, \qquad (2.5.46)$$

where θ_1 is the incident angle, b is the incident beam size and B is diffracted beam size. The ratio of B to b is a measurement of the geometric aberration and will be referred to as the defocusing factor. In principle, defocusing occurs only when B/b is larger than 1. The reflected beam is actually focused to the detector when $\theta_2 < \theta_1$. The defocusing effect occurs when $\theta_2 > \theta_1$ and the defocusing factor increases with increasing θ_2 or decreasing θ_1. The maximum defocusing appears at $\theta_2 = 90^\circ$. For the θ–2θ configuration, the incident angle ω ($= \theta_1$) is used in the equation.

For B-B geometry with a divergent slit and receiving slit of the same size the defocusing factor is always 1. With a 2D detector the defocusing factor varies with the 2θ angle. If a large 2θ range is measured on a flat sample in reflection mode, it is always desirable to collect several frames at different incident angles for each 2θ range so as to improve the 2θ resolution. A cylindrical detector may collect a diffraction pattern over a large 2θ range (Gelfi *et al.*, 2005). However, the defocusing effect prevents it from being used for a large 2θ range for a flat sample. Fig. 2.5.17 compares the effect for a flat detector and a cylindrical detector. Fig. 2.5.17(*a*) shows a cylindrical detector being used to collect a diffraction pattern from a flat sample for a 2θ range of 5 to 80°. The incident angle must be kept at 5° or lower. Fig. 2.5.17(*b*) shows a flat detector being used to collect the diffraction pattern over the same 2θ range. In order to minimize the defocusing effect, the data collection is done at four different incident angles (5, 15, 25 and 35°) with four corresponding detector swing angles (10, 30, 50 and 70°). Fig. 2.5.17(*c*) compares the defocusing factors of the two configurations. The horizontal dot-dashed line with defocusing factor $B/b = 1$ represents the situation with B-B geometry. The defocusing factor continues to increase with 2θ angle up to $B/b = 11$ for cylindrical detector. That means that the 2θ resolution would be 10 times worse than for the B-B geometry. For the diffraction pattern collected with a flat detector in four steps, the defocusing factor fluctuates above 1, with the worst value being less than 3. Another approach to avoiding defocusing is to collect the diffraction pattern in transmission mode. There is no defocusing effect in transmission when the incident beam is perpendicular to the sample surface. Therefore, the transmission pattern has significantly better 2θ resolution. Transmission-mode diffraction also has other advantages. For instance, the air scattering from the primary beam may be blocked by a flat sample, therefore lowering the background from air scattering. However, transmission-mode diffraction data can only be collected from samples with limited thickness, and the maximum scattering intensity is achieved at low 2θ angles with a sample thickness of $t = 1/\mu$, where μ is the linear absorption coefficient. The scattering intensity drops dramatically when the thickness increases.

2.5.4.1.4. *Sampling statistics*

In powder X-ray diffraction, the number of crystallites contributing to each reflection must be sufficiently large to generate reproducible integrated peak intensities (see Chapter 2.10). A larger number of contributing crystallites gives better precision or sampling statistics (also referred to as particle

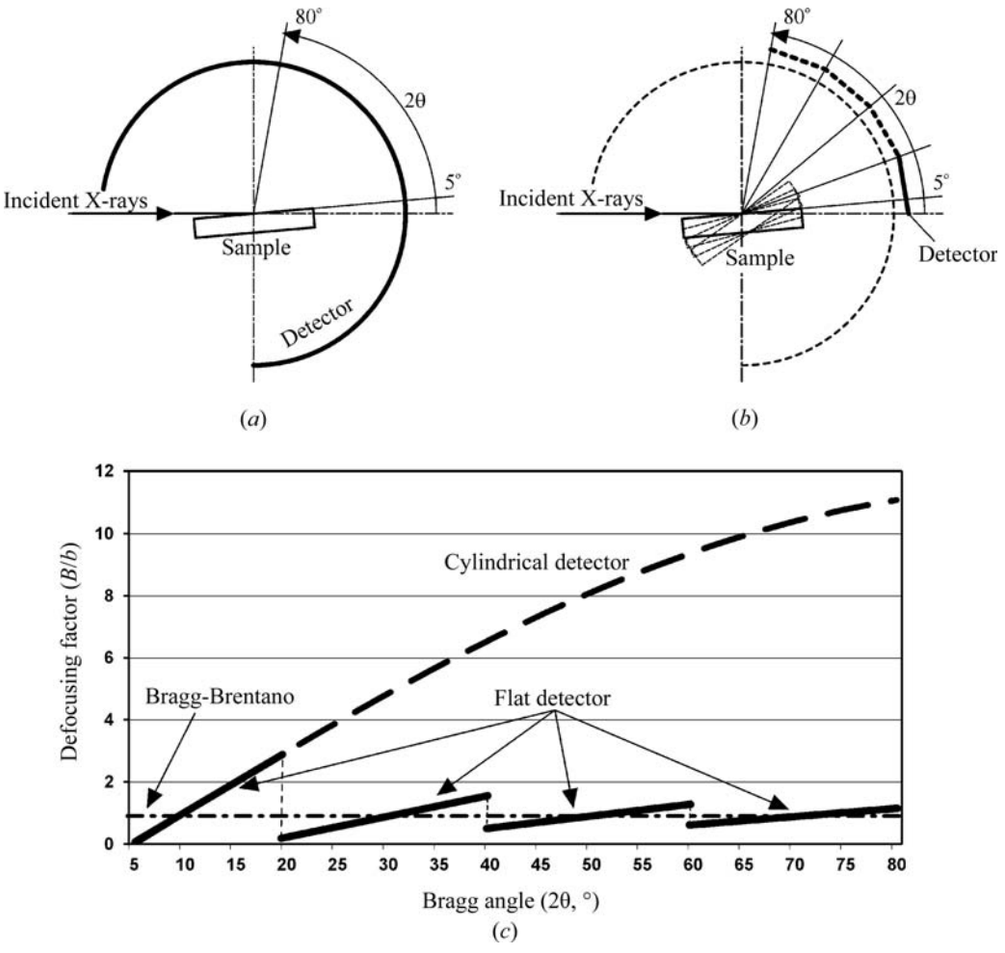

Figure 2.5.17
Defocusing effects: (*a*) cylindrical detector; (*b*) flat detector at various incident angles and detector swing angles; (*c*) comparison of defocusing factors.

statistics). Sampling statistics are determined by both the structure of the sample and the instrumentation. For a powder sample in which the crystallites are perfectly randomly oriented, the number of contributing crystallites for a diffraction peak can be given as

$$N_s = p_{hkl}\frac{Vf_i}{v_i}\frac{\Omega}{4\pi}, \tag{2.5.47}$$

where p_{hkl} is the multiplicity of the diffracting planes, V is the effective sampling volume, f_i is the volume fraction of the measuring crystallites (f_i = 1 for single-phase materials), v_i is the volume of individual crystallites and Ω is the angular window of the instrument (given as a solid angle). The multiplicity term, p_{hkl}, effectively increases the number of crystallites contributing to the integrated intensity from a particular set of (hkl) planes. The volume of individual crystallites, v_i, is an average of various crystallite sizes. The combination of the effective sampling volume and the angular window makes up the instrumental window, which determines the total volume of polycrystalline material making a contribution to a Bragg reflection. For 2D-XRD, the instrumental window is not only determined by the incident beam size and divergence, but also by the detective area and the sample-to-detector distance (γ angular coverage).

In B-B geometry, the effective irradiated volume is a constant,

$$V_{\rm BB} = A_o A_{\rm BB} = A_o/2\mu, \tag{2.5.48}$$

where A_o is the cross-section area of the incident beam measured on the sample surface, $A_{\rm BB} = 1/(2\mu)$ is the transmission coefficient for B-B geometry, and μ is the linear absorption coefficient. For 2D-XRD, the effective volume is given as

$$V = A_o A = A_o T/2\mu, \tag{2.5.49}$$

where A is the transmission coefficient and T is the transmission coefficient with B-B normalization for either transmission or reflection as given previously.

The angular window is given as a solid angle. The incident beam has a divergence angle of β_1 within the diffraction plane and β_2 in the perpendicular direction. The angular window corresponding to the incident-beam divergence is given by

$$\Omega = \beta_1\beta_2/\sin\theta \text{ or } \Omega = \beta^2/\sin\theta \text{ if } \beta = \beta_1 = \beta_2. \tag{2.5.50}$$

For 2D-XRD, the angular window is not only determined by the incident-beam divergence, but also significantly increased by γ integration. When γ integration is used to generate the diffraction profile, it actually integrates the data collected over a range of various diffraction vectors. Since the effect of γ integration on sampling statistics is equivalent to the angular oscillation on the ψ axis in a conventional diffractometer, the effect is referred to as virtual oscillation and $\Delta\psi$ is the virtual oscillation angle. In conventional oscillation, mechanical movement may result in some sample-position error. Since there is no actual physical movement of the sample stage during data collection, virtual oscillation can avoid this error. This is crucial for microdiffraction. The angular window with the contributions of both the incident-beam divergence and the virtual oscillation is

$$\Omega = \beta\Delta\psi = 2\beta\arcsin[\cos\theta\sin(\Delta\gamma/2)], \tag{2.5.51}$$

where β is the divergence of the incident beam. While increasing the divergence angle β may introduce instrumental broadening which deteriorates the 2θ resolution, virtual oscillation improves sampling statistics without introducing instrumental broadening.

In the cases of materials with a large grain size or preferred orientation, or of microdiffraction with a small X-ray beam size, it can be difficult to determine the 2θ position because of poor counting statistics. In these cases, some kind of sample oscillation, either by translation or rotation, can bring more crystallites into the diffraction condition. Angular oscillation is an enhancement to the angular window of the instrument. The effect is that the angular window scans over the oscillation angle. Any of the three rotation angles (ω, ψ, φ) or their combinations can be used as oscillation angles. Angular oscillation can effectively improve the sampling statistics for both large grain size and preferred orientation. As an extreme example, a powder-diffraction pattern can be generated from single-crystal sample if a sufficient angular window can be achieved by sample rotation in such as way as to simulate a Gandolfi camera (Guggenheim, 2005). Sample oscillation is not always necessary if virtual oscillation can achieve sufficient sampling statistics.

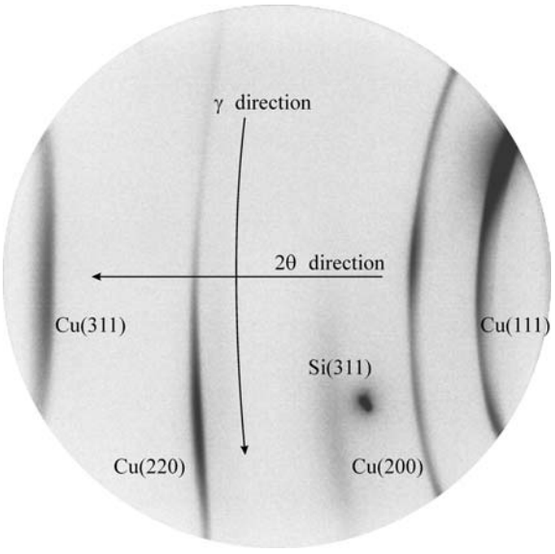

Figure 2.5.18
Diffraction frame collected from a Cu film on an Si substrate showing intensity variation along γ due to texture.

2.5.4.2. *Texture analysis*

Most natural or artificial solid materials are polycrystalline, consisting of many crystallites (also called grains) of various sizes, shapes and orientations. When the orientations of the crystallites in a material have a random distribution, it presents isotropic properties. The anisotropic orientation distribution of crystallites is referred to as preferred orientation or texture. Depending on the degree of the preferred orientation, a sample is referred to as having a weak, moderate or strong texture. Many electrical, optical or mechanical properties of materials are affected or determined by their texture. The determination and interpretation of textures are therefore of fundamental importance in materials science and technology (Bunge, 1983).

When a conventional X-ray diffractometer with a point detector is used for texture measurement, the crystallite orientation distribution in one direction is measured at a time, and full texture information is measured by rotating the sample to all the desired orientations. When a two-dimensional X-ray diffraction system is used for texture measurement, the orientation distributions of several crystallographic planes over a range of angles can be measured simultaneously so as to get better measurement results in a shorter data-collection time (Smith & Ortega, 1993; Blanton, 1994; Bunge & Klein, 1996; Helming *et al.*, 2003; Wenk & Grigull, 2003; He, 2009). The orientation relationships between different phases or between different layers of thin films and substrates can also be easily revealed. The texture effect may be observed and evaluated directly from the 2D diffraction frames without data processing.

2.5.4.2.1. *Pole density and pole figures*

XRD results from an 'ideal' powder in which the crystallites are randomly oriented normally serve as a basis for determining the relative intensity of each diffraction peak. The deviation of the grain orientation distribution of a polycrystalline material from that of an ideal powder is measured as texture. The pole figure for a particular crystallographic plane is normally used to represent the texture of a sample. Assuming that all grains have the same volume, each 'pole' represents a grain that satisfies the Bragg condition. The number of grains satisfying the Bragg condition at a particular sample orientation can be larger or smaller than the number of grains for an ideal sample, and likewise for the integrated intensity of that peak. The measured 2D diffraction pattern contains two very important parameters at each γ angle: the partially integrated intensity I and the Bragg angle 2θ. Fig. 2.5.18 shows a 2D frame for a Cu thin film on an Si wafer collected with a microgap 2D detector. It contains four Cu lines and one Si spot. The diffraction intensity varies along γ because of the anisotropic pole-density distribution. For each diffraction ring, the intensity is a function of γ and the sample orientation (ω, ψ, φ), *i.e.* $I = I(\gamma, \omega, \psi, \varphi)$.

Plotting the intensity of each (hkl) line with respect to the sample coordinates in a stereographic projection gives a qualitative view of the orientation of the crystallites with respect to a sample direction. These stereographic projection plots are called pole figures. As is shown in Fig. 2.5.19(a), the sample orientation is defined by the sample coordinates S_1, S_2 and S_3. For metals with rolling texture, the axes S_1, S_2 and S_3 correspond to the transverse direction (TD), rolling direction (RD) and normal direction (ND), respectively. Let us consider a sphere with unit radius and the origin at O. A unit vector representing an arbitrary pole direction starts from the origin O and ends at the point P on the sphere. The pole direction is defined by the radial angle α and azimuthal angle β. The pole density at the point P projects to the point P' on the equatorial plane through a straight line from P to the point S. The pole densities at all directions are mapped onto the equatorial plane by stereographic projection as shown in Fig. 2.5.19(b). This two-dimensional mapping of the pole density onto the equatorial plane is called a pole figure. The azimuthal angle β projects to the pole figure as a rotation angle about the centre of the pole figure from the sample direction S_1. When plotting the pole density into a pole figure of radius R, the location of the point P' in the pole figure should be given by β and

$$r = R\tan\left(\frac{\pi}{4} - \frac{\alpha}{2}\right) = R\tan\frac{\chi}{2}. \qquad (2.5.52)$$

For easy computer plotting and easy angular readout from the pole figure, the radial angle α may be plotted on an equally spaced angular scale, similar to a two-dimensional polar coordinate system. Other pole-figure mapping styles may be used, but must be properly noted to avoid confusion (Birkholz, 2006).